

Microstructural evolution in creep exposed IN617

R. Krishna, S.V. Hainsworth, S.P.A. Gill, A. Strang and H. V. Atkinson

Department of Engineering, University of Leicester, University Road, Leicester, LE1 7RH, UK

Abstract

Inconel alloys are currently being investigated for high temperature applications such as HP and IP valve chest and rotor forgings in advanced steam power plant operating at temperatures of 700°C and above. One of the preferred alloys for these components is IN617. This is a solid solution strengthened austenitic Ni-based alloy containing ~23% Cr, 12% Co, and 9% Mo with small additions of Ti and Al which can contribute some additional precipitation strengthening. In the solution treated condition, the microstructure consists of equiaxed austenite containing $M_{23}C_6$ at the grain boundaries and occasional TiN particles within the matrix. Owing to high temperature exposure and the creep deformation processes that occur in-service, evolution of the microstructure occurs in the form of precipitation, precipitate coarsening and recovery effects. This paper discusses microstructural evolution occurring in this alloy in samples that have been exposed to temperatures up to 700°C and for durations up to 45,000 hours using advanced FEGSEM, TEM and XRD techniques.

Keywords: IN617; Solid-solution strengthening; Hardness; FEGSEM; Intergranular fracture; Gamma prime (γ'); TEM.

1. Introduction

In order to increase the thermal efficiency of power plants and reduce harmful emissions of gases such as SO_x , NO_x and CO_x to atmosphere, there is a need to raise the operating temperature of power plant [1-7]. The current working steam temperatures of most efficient power plants are now in the range of 600°C-650°C with steam pressures of 30 MPa and it is expected that temperatures will rise up to 700°C and above to obtain the necessary high thermal efficiencies. In order to meet the material requirements for creep resistance, microstructural stability, fatigue, fracture toughness, corrosion and oxidation resistance, Ni-based superalloys are being investigated for critical components such as the HP/IP valve chest, rotor forgings, blades, pipes, tubes, headers etc. [7-9].

IN617 (Ni-23Cr-12Co-9Mo) is the one of the preferred structural materials from the nickel-based superalloys family to meet the temperature capability challenge for future generation steam turbines and their components. The high temperature capability of IN617 arises from good mechanical strength at elevated temperature, long term metallurgical stability, good creep rupture strength for long term operation, and excellent corrosion and oxidation resistance in aggressive operating environments [10-12].

IN617 is a solid solution strengthened alloy. It also contains a fine dispersion of ordered intermetallic precipitates (resistant to coarsening) which are embedded in the disordered solid-solution strengthened austenitic matrix phase [13, 14]. **The alloy's high temperature strength is determined by the presence of intermetallic precipitate (gamma prime) in the solid solution rather than get precipitated out from the solid solution.** Secondary hardening arises from localized precipitation after ageing heat-treatment in a solution-annealed condition and during longer exposure at service temperature. Various alloying solute elements (Cr, Co, Mo, Al, Ti, Fe) are responsible for elevated temperature structural and mechanical performance [15, 16]. The optimal solute amounts of Al and Ti play a major role in formation of the main coherent hardening phase; the ordered $L1_2$ intermetallic gamma prime (γ' ; $Ni_3(Al, Ti)$). γ' precipitates coherently in a nickel-rich fcc γ matrix and acts as a barrier to the movement of dislocations.

Solutes like Cr, Co, Mo provide solid solution strengthening to the austenitic matrix and contribute to secondary hardening by carbide precipitation. The precipitation of inter- and intra- grain boundary carbides such as $M_{23}C_6$, M_6C , MC , nitrides and carbo-nitrides ($M(C, N)$), within the grains and at grain boundaries, at service temperature is a common phenomena in Ni-based alloys [21-24]. After extended exposure to high temperatures and mechanical stresses in aggressive environmental conditions, the mechanical properties of the alloys degrade, owing to changes that occur in their microstructures. The degradation of properties can ultimately lead to catastrophic failure of components in service [17-24].

The work in this paper investigates the effect of stresses and temperatures (650°C and 700°C) that are relevant to conventional power plant. Precipitate evolution has been studied with scanning electron and transmission electron microscopy. The precipitates that are observed experimentally are compared to phase predictions from Thermo-calc. The evolution of mechanical properties has been investigated using hardness testing. Finally, the creep failure mechanisms of the different samples have been investigated by observation of the fracture surfaces and cross-sections through the fracture by scanning electron and optical microscopy respectively.

2. Materials and experimental procedures

Standard creep rupture specimens were prepared from a solution annealed forged rod of IN617 (Ni-23Cr-12Co-9Mo-1Al-0.48Ti-0.06C). The complete nominal chemical composition of ‘as received’ IN617 is given in Table 1. The ASTM grain size number and hardness of the ‘as received’ specimen was 5.0 and 186.6±5 H_v/20 respectively.

Table 1: Chemical composition of IN617 (in weight %)

Elements	Ni	Cr	Mo	Co	Al	Ti	Fe	C	Si	W
Wt %	Bal.	22.8	9.0	11.9	1.15	0.48	0.35	0.06	0.05	0.02
Elements	Mn	Cu	Zr	P	V	N	Nb	S	B	
Wt %	0.02	0.013	0.005	0.005	0.005	0.004	0.003	0.001	0.0002	

The solution-annealed forged rods were given two stage heat treatments, solutionization: 1100°C/3 Hrs/WQ; followed by ageing: 670°C/ 10 Hrs/ AC; before being creep-tested. Creep rupture tests were carried out at 650°C and 700°C in air by ALSTOM, Rugby, UK. The creep test conditions and durations to failure along with their corresponding reduction in area after testing of the samples investigated in this study are shown in table 2.

Table 2: Creep-test conditions

Alloy	Specimen ID	Temp.	Duration* (h)	RA%
IN617 (Solution-annealed condition)	1 (T0154)	700 °C	32 000	1.0
	2 (T0151)	700 °C	4000	12.5
	3 (T0008)	650 °C	45 000	0.8
	4 (T0003)	650 °C	574	2.4

*All creep tests were continued till rupture.

Microstructural evolution investigations were conducted on head (stress free regions) and gauge length of ‘as received’ and creep-ruptured specimens of IN617 using optical metallography (OM), scanning electron microscopy (FEGSEM), transmission electron microscopy (TEM) and X-ray diffraction.

Vickers hardness tests were conducted using a 20kgf load on longitudinal cross-sections of the creep fractured specimens.

Metallographic specimens were prepared from the head and gauge length of each creep specimen. Specimens were mounted in phenolic resin, polished, and etched in glyceresia which is a mixture of hydrochloric acid, glycerol and nitric acid in a 3:2:1 ratio.

Electron backscattered diffraction orientation images were obtained using an HKL Channel 5 EBSD system attached to an FEI Sirion 200 field emission gun scanning electron microscope. The accelerating voltage used was 20kV. A step size of 4.3 μ m was used. Full automatic indexing of the microstructure was obtained using proprietary software: Flamenco was used for image acquisition and indexing and Tango was used for orientation maps. Indexing was performed using an fcc nickel structure with a lattice parameter $a=0.352$ nm. Typical indexing rates were 97-98%.

3mm thin foils of specimens mechanically polished to 40-60 μ m thickness were prepared from the gauge length of the creep tested specimens for transmission electron microscopy. Final electro-polishing to perforation was performed with twin-jet electro polishing (Model: 120; Fischione Instrument, USA) using an electro-polishing mixture of perchloric acid (HClO₄) and methanol (MeOH) in 1:4 ratios at 35 V and -40°C. The specimens were then examined using a JEOL (Japan) JEM 2100 Model LaB₆ TEM with an operating voltage of 200 kV.

Thermodynamic calculations were performed to predict the phase stability in the alloy at different temperatures using Thermo-Calc software [25].

3. Results and discussion

3.1 *As-received microstructure of IN617*

The initial microstructure of the solution treated and aged alloy is shown in figure 1. The optical micrograph shows that the alloy has an equiaxed austenitic grain structure with average size ranges from 90-150 μ m. Twinning is apparent in a number of the grains. Secondary precipitate phases are found both intra- and inter-granularly. Figure 2 shows scanning electron microscope images with particles of less than 1 μ m size situated at intra- and inter-granular regions and some larger particles within the grains. EBSD analysis showed that the grains were randomly oriented with no preferred texture. The average grain size from EBSD was 115 μ m.

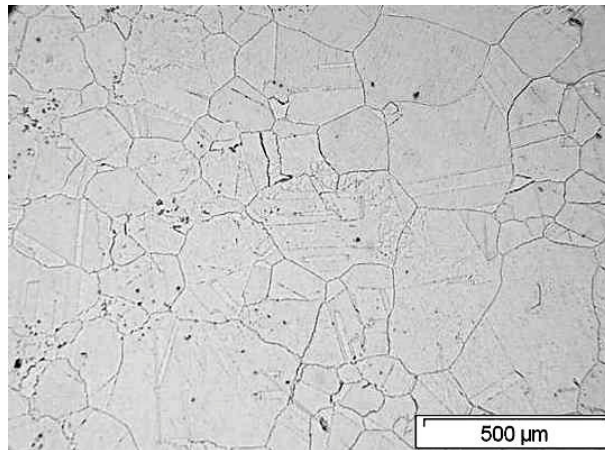


Figure 1: Optical micrograph showing the solution treated and aged ‘as-received’ condition of IN617.

Energy dispersive X-ray microanalyses of the ‘as-received’ IN 617 alloy showed only two types of precipitates: (i) titanium enriched precipitates, and (ii) chromium enriched precipitates. Typical analyses of these particles are shown in figure 3. The morphology of the precipitates was found to vary quite considerably from the irregular geometries to the more defined cubic geometry as shown in

micrograph in figure 3a & figure 3b. Particles were found both intra- and inter-granularly and the size varied from <math><1\mu\text{m}</math> through to $10\mu\text{m}$.

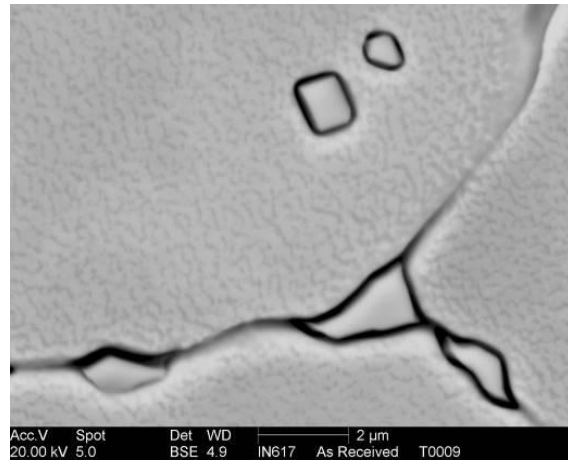
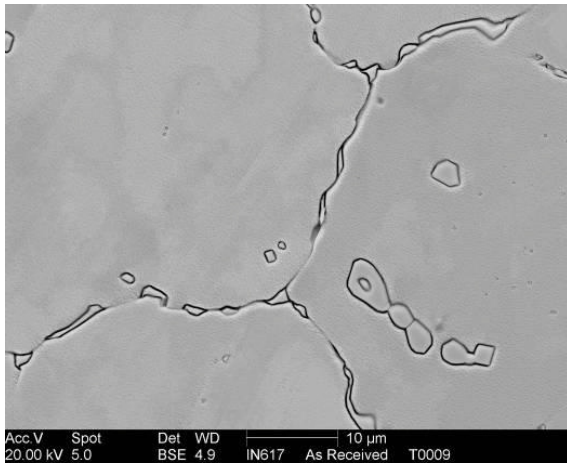


Figure 2a: Grain boundary and intra-granular precipitates in the as-received alloy.

Figure 2b: Higher magnification image of figure 2a.

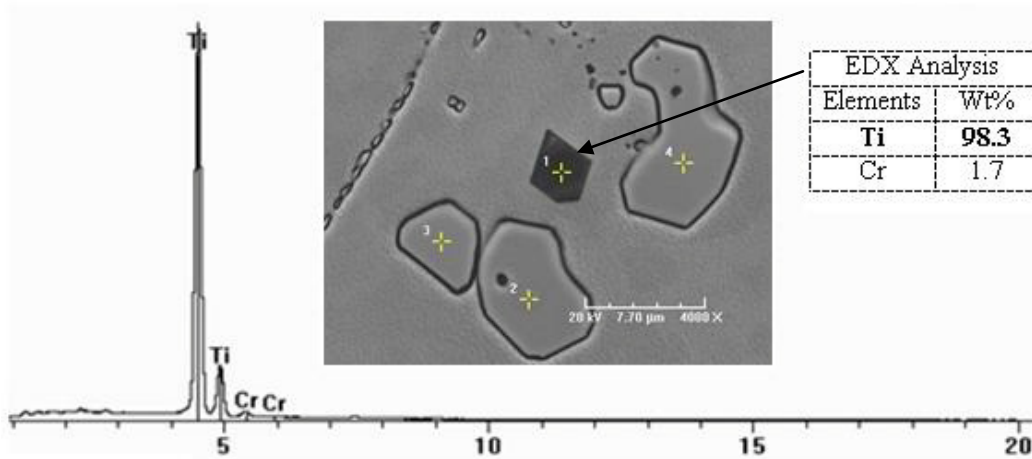


Figure 3a: Energy dispersive X-ray analysis of a Ti-rich precipitate found inside the grain in the as-received sample

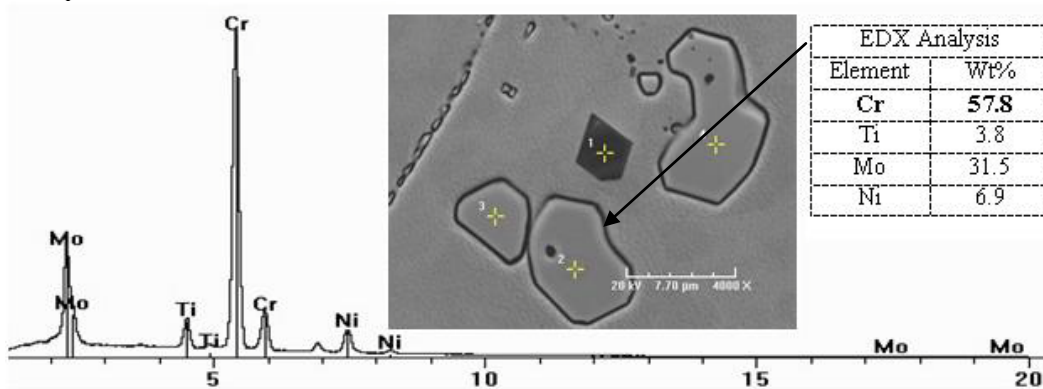


Figure 3b: Energy dispersive X-ray analysis of a Cr-rich precipitate found inside the grain in the as-received sample.

3.2 Thermodynamic calculations of equilibrium phases

Thermo-calc software [25] has been used to calculate the expected phases present in IN617 under equilibrium conditions. The expected phases at temperatures of 650° and 700° C are gamma prime (γ'), $M_{23}C_6$ (Cr-enriched), Mu (μ) phase (Mo-enriched), TiN (Ti-enriched) and gamma matrix (γ). The phase mole fractions for differing temperatures are shown in figure 4. The nitrogen content in the alloy has an important effect on the formation of both γ' and TiN. Figure 5a shows the effect of nitrogen content in the alloy on its strengthening phases of γ' and TiN. At low weight % nitrogen, the N content does not have significant effect on the γ' fraction. However, at increasing nitrogen contents, the nitrogen is critical in determining the volume fraction of γ' . Figure 5b shows that titanium starts to diffuse out of the gamma prime to form titanium nitride, with an increase in nitrogen content. Below 0.08 wt% of nitrogen, γ' is present in a greater weight percent than titanium nitride and above 0.08 wt% of nitrogen, titanium nitride is the predominant phase.

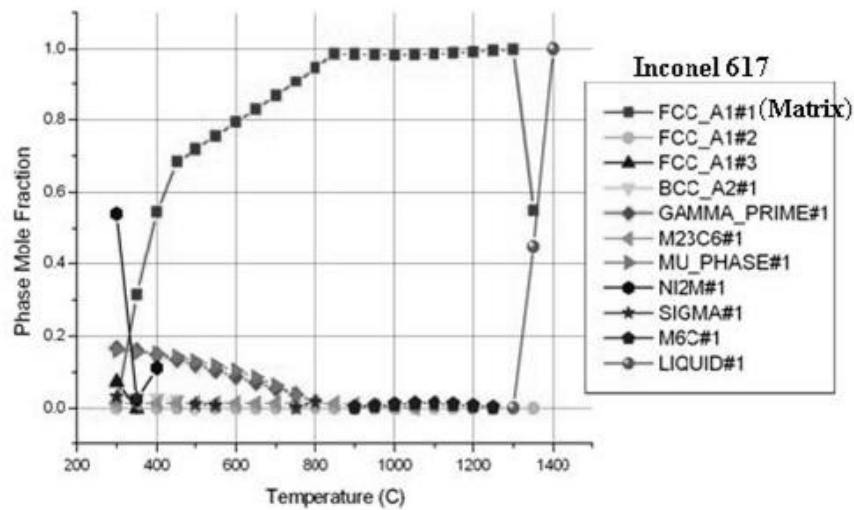


Figure 4: Thermo-calc predictions for the equilibrium phase mole fractions as a function of temperature.

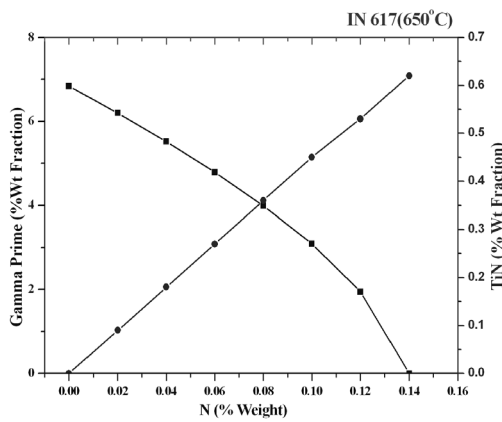


Figure 5a: Variation of gamma prime (■) content and TiN (●) content as function of nitrogen concentration.

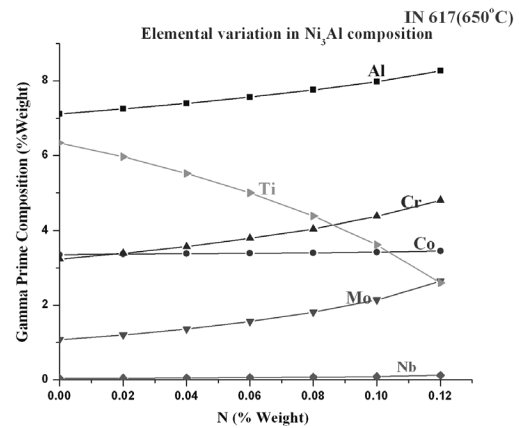


Figure 5b: Composition of γ' as a function of nitrogen concentration.

3.3 Microstructural evolution

Table 3 shows the major precipitates found in the gauge length after creep exposure.

Table 3: Precipitate evolution after creep exposure

Specimen ID	Temp.	Duration* (h)	RA%	Precipitate type
T0154	700 °C	32 000	1.0	Carbides, nitrides and carbo-nitrides, of Cr-, Ti- and Mo-enriched phases, intra- and inter-granularly
T0151	700 °C	4000	12.5	Carbides, nitrides and carbo-nitrides, of Cr-, Ti- and Mo-enriched phases, intra- and inter-granularly
T0008	650 °C	45 000	0.8	Extensive precipitation of Ti-, Cr- and Mo-enriched precipitates throughout the matrix
T0003	650 °C	574	2.4	Extensive precipitation of Ti- and Cr-enriched particles on grain boundaries and twin boundaries

The precipitates found in T0154 included the Mo-rich μ -phase which is shown in greater detail in figure 6. The grain size of all creep exposed samples was found to be larger than the ‘as-received’ alloy, typically in the region of 150-200 μ m as can be seen in figure 7.

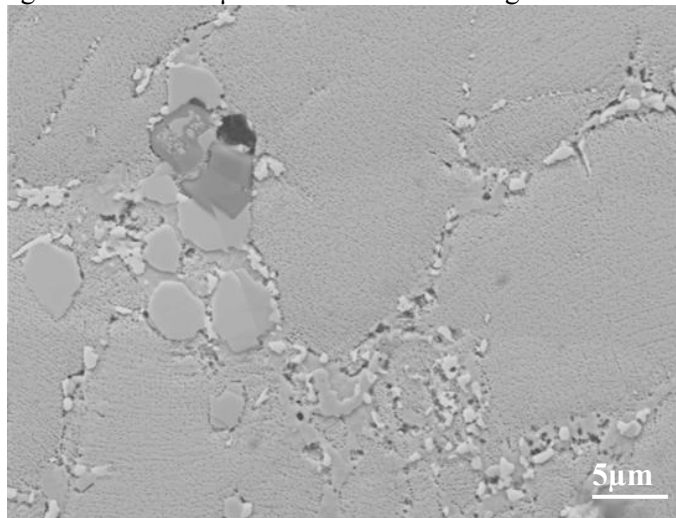


Figure 6: Scanning electron micrograph of sample T0154 exposed to 700C for 32,000 hours. The μ -phase is the white phase seen at the grain boundaries.

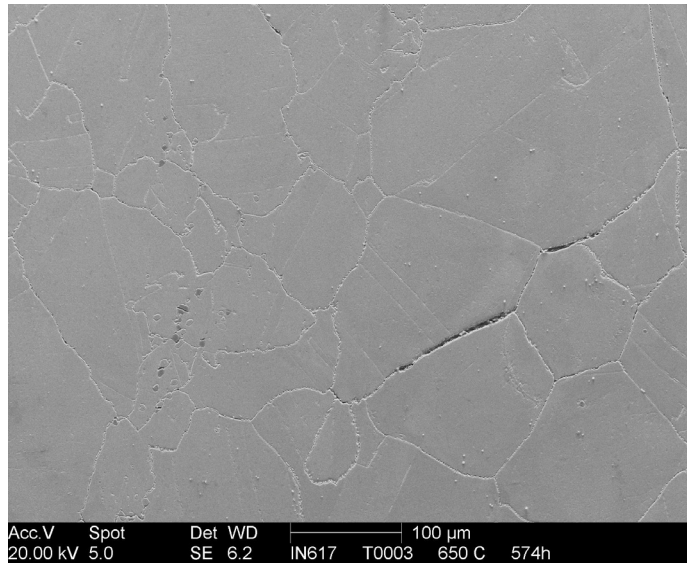


Figure 7: Scanning electron micrograph showing that the average grain size in the creep-exposed samples has increased from an average size of 90-150 μm to 150-200 μm . This micrograph is from sample T0003 which was exposed to 650 $^{\circ}\text{C}$ for 574 hours.

3.4 Hardness profiles for creep-ruptured IN617 alloy specimens at 600 $^{\circ}\text{C}$ and 700 $^{\circ}\text{C}$

Hardness was measured at 2mm intervals along the head and gauge length of the longitudinally-sectioned specimens of the creep-exposed samples. The results of the hardness testing are shown in figure 8. Each hardness value is an average of three indentations across the diameter of the specimen. The error bars show the 90% confidence limits.

From figure 8, it can be seen that for all the samples the hardness in the head region of the specimen, where it may be assumed that the major effect on the sample is from the thermal effects with minimal effect from stress, is lower than the hardness measured along the gauge length. The head hardness is least for the sample exposed at 650 $^{\circ}\text{C}$ for only 574 hours. For all the samples, the hardness of the heads has increased substantially above that of the ‘as-received’ sample which had a hardness of 186.6Hv.

Specimen T0008, which ruptured after 45,000 hours exposure at 650 $^{\circ}\text{C}$, had the highest average value of Vickers hardness in the gauge at 353 Hv. This specimen showed very little reduction in area (0.8%). When the microstructure was analysed, the specimen showed extensive precipitation of Ti-, Cr-, and Mo-enriched precipitates had occurred throughout the matrix. T0151 and T0003 showed the next greatest increase in hardness with T0154 showing the least difference between head and gauge hardness. For this sample, it may be that internal damage from coarsening of the γ' [$\text{Ni}_3(\text{Al}, \text{Ti})$] phase, grain growth and grain boundary creep voiding has occurred. Internal damage of this nature does not lead to dimensional changes in the specimen but results in decreases in mechanical properties such as hardness and creep strength [26, 27].

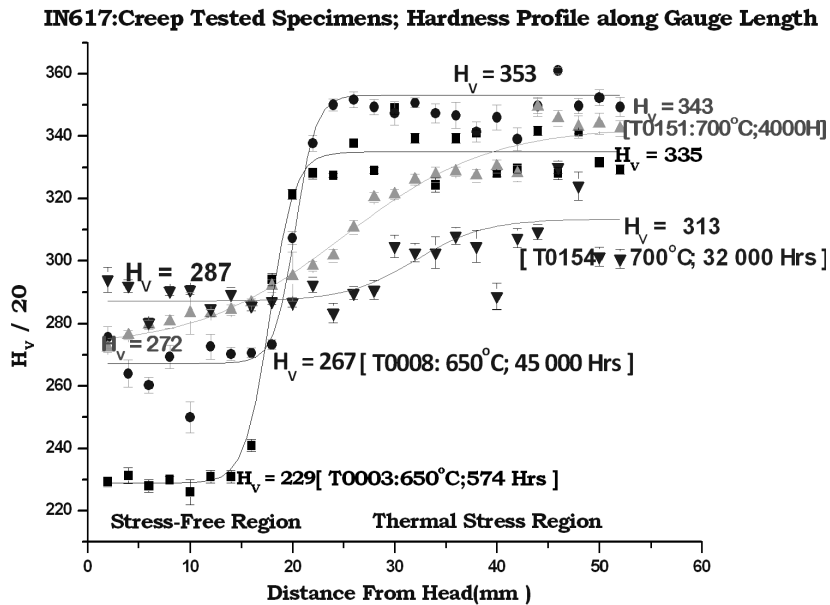


Figure 8: Hardness versus distance from head for the creep-exposed samples at 650°C and 700°C.

3.5. Fractography of creep-exposed specimens

The creep failure mechanisms of the failed specimens have been analyzed using scanning electron microscopy and optical microscopy. Figure 9 shows a montage of scanning electron microscopy images from the fracture surface of T0008 which had been exposed at 650°C for 45,000 hours creep duration. The failure mechanism for this specimen was intergranular failure by decohesion of the grain boundaries.

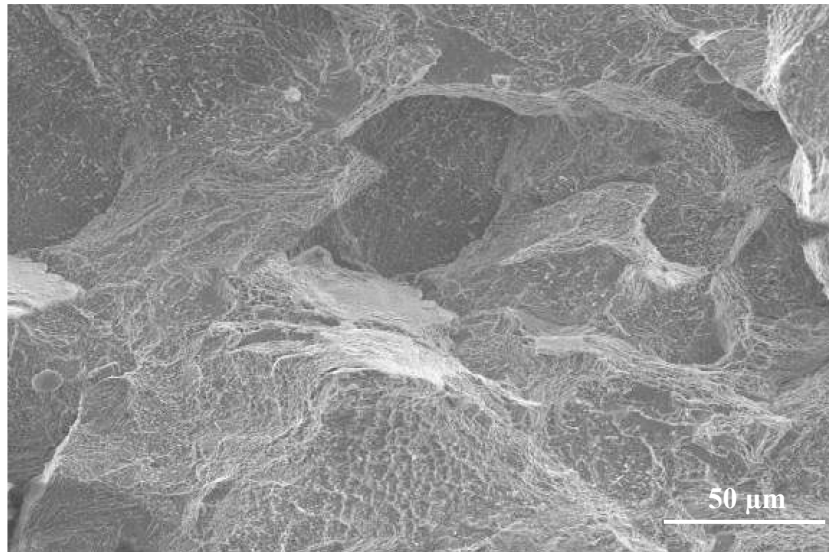


Figure 9: Intergranular creep failure of T0008 exposed at 650 °C for 45,000 hours duration.

Intergranular creep fracture involves the nucleation, growth and subsequent linking of voids at grain boundaries to form two differing types of cavities, wedge type cavities and isolated type cavities. Wedge type cavities are associated with cracking at grain boundary triple points and form by grain

boundary sliding. The formation of cavities is controlled by a diffusion-controlled process. Figure 8 shows an example of triple point wedge cracking in T0151 which has been exposed at 700°C for 4000 hours creep duration.

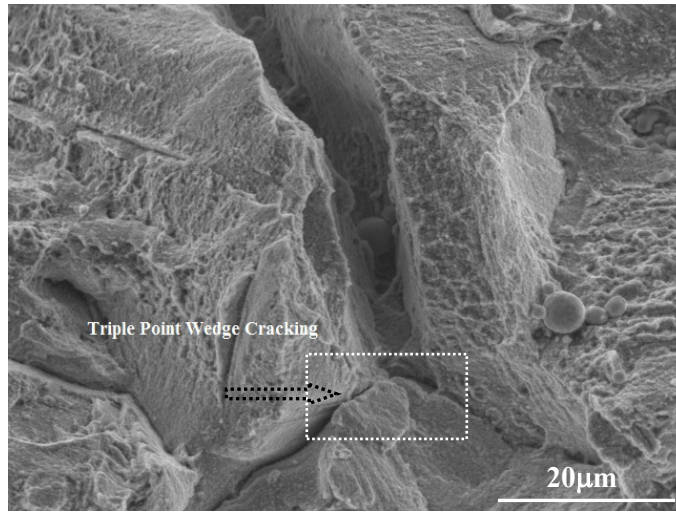


Figure 10: Triple point wedge cracking in T0151 exposed at 700°C for 4000 hours duration.

The failure mechanisms of the samples were further confirmed by optical microscopy of polished cross-sections. Figure 11 shows further confirmation of wedge cracking and decohesion of the grain boundaries in T0003 which was exposed at 650C for 574 hours. The direction of loading is shown by the dotted arrow.

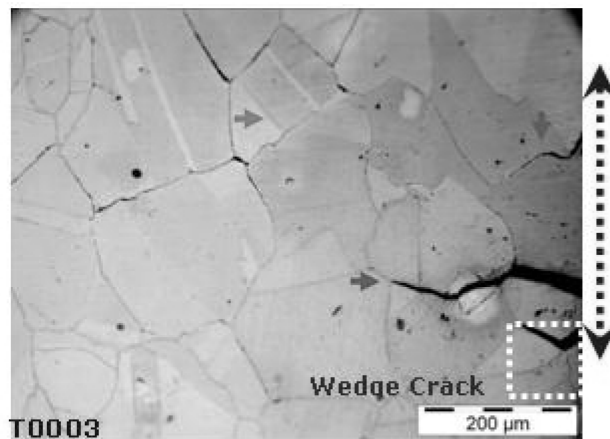


Figure 11: Optical micrograph showing wedge cracking and grain boundary decohesion in T0003.

The creep fracture mechanism for both samples exposed at 650C was found to be intergranular in nature. For the specimens that were creep exposed at 700C, there was some evidence for a contribution from transgranular cracking in addition to the intergranular failure.

3.6. Transmission electron microscopy

Transmission electron microscopy was conducted to identify the morphology and distribution of the gamma prime (γ') in creep exposed specimen at 650°C. The γ' - phase was found to have a spherical morphology of size ranging from 10 – 15 nm, periodically spaced at 5 nm distance (see figure 12).

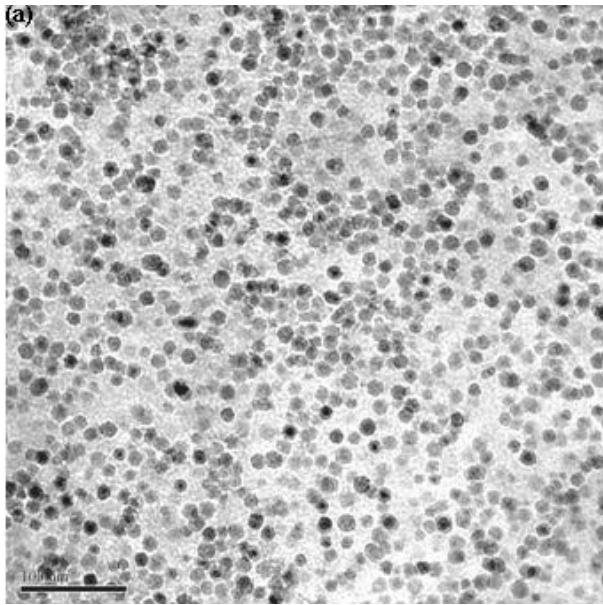


Figure 12a: Bright field transmission electron micrograph of gamma prime (γ') [$\text{Ni}_3(\text{Al}, \text{Ti})$: FCC $L1_2$ Space Group] of 10 – 15 nm size, spherical morphology, finely dispersed at equi-spaced distance and coherent with austenitic γ matrix.

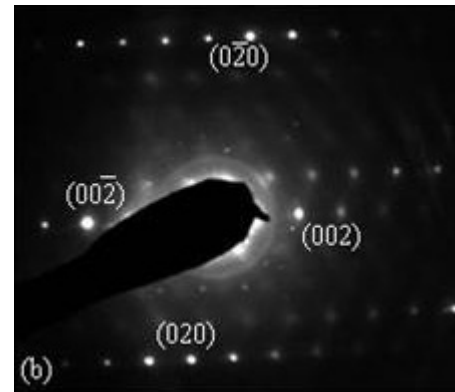


Figure 12b: SADP showing crystallographic planes from the matrix γ and γ' phase

4. Discussion

Predictions from Thermo-calc show that the equilibrium phases of IN617 at 650 and 700 should be gamma prime (γ'), $M_{23}C_6$ (Cr-enriched), μ (μ) phase (Mo-enriched), TiN (Ti-enriched) and gamma matrix (γ). Our experimental observations have confirmed the presence of these phases, but μ -phase was only observed for the specimen that had been creep-exposed to 45,000 hours. At temperatures and creep durations lower than this, no μ -phase was observed. γ' particles were found to be of fine size and uniformly distributed throughout the matrix. The estimation of the volume fraction of γ' is difficult to establish owing to the difficulties of estimating the volume of material analysed in TEM cross-sections. Further work is continuing in this area to allow reliable quantification of γ' content in the differing creep-exposed specimens.

The hardness of all creep exposed specimens was higher than for the 'as-received' solution treated and aged specimen. The thermally exposed head regions of the samples had lower hardnesses than the gauges that had been exposed to both stress and temperature. All samples showed an extensive network of precipitates in both the grain boundaries that were decorated with contiguous precipitates that were mainly Cr-rich in nature, and the grains themselves. Precipitates of different types were found to have varying morphology and there was no straight-forward relationship between morphology of precipitates and composition. The rises in hardness observed in the head and gauge of the specimens are attributed to secondary hardening effects from the precipitates and the γ' dispersed throughout the matrix [28]. It is possible that the drop in hardness relative to the other samples for T154 which was exposed at 700 for 32,000 hours may be owing to coarsening of the γ' although further work is required to confirm this point.

Creep failure occurred usually by an intergranular creep mechanism although for higher temperature creep exposure there was some evidence of a transgranular contribution to the creep failure mechanism.

5. Conclusions

The microstructure of IN617 has been studied after long-time exposure to temperatures of 650°C to 700°C. Optical microscopy, scanning electron microscopy and transmission electron microscopy have been used to study the phase precipitation and microstructural evolution in IN617. The experimental observations are summarized as follows:

- i. The precipitates observed in the samples investigated here broadly agreed with Thermo-calc predictions for temperatures of 650°C and 700°C, but μ phase was only observed after long creep exposures at 700°C.
- ii. The grains were randomly oriented in 'as received' IN617 alloy. The average grain size of the 'as received' IN617 was 115 μm , but for the creep exposed IN617 specimen the average grain size varies from 150-200 μm .
- iii. The major precipitates at temperature below 700°C were Cr-enriched (M_{23}C_6) and Ti-enriched (TiN). At 700°C the major precipitates includes Mo-enriched (μ phase) with Cr-enriched (M_{23}C_6) and Ti-enriched (TiN). At 700°C, the precipitates were found to precipitate in large proportions at twin and grain boundaries, but otherwise, precipitates were randomly distributed throughout the matrix.
- iv. The creep fracture mode at 650°C is predominantly intergranular in nature. The accumulation of high stress concentration regions like cavities and wedge cracks, in materials under stress and high service temperature, leads to permanent failure. At 700°C the fracture mode is not purely intergranular. Extensive grain boundary cavitation was observed at high temperature. Creep cracks always initiated at grain boundary triple points, grain boundary precipitates and polygrain junctions.

6. Acknowledgements

The authors would like to thank ALSTOM for supplying creep exposed samples and wish to acknowledge the Department of Trade and Industry (DTI) for providing financial support to carry out this work.

7. References

- [1] Viswanathan, R., Gandy, D., Coleman, K. (Editors). Advances in Materials Technology for Fossil Power Plants (Proceedings of the Fourth International Conference, EPRI). ASM International, Jan 2005.
- [2] Vanstone, R.W. Advanced (700 °C) pulverised fuel power plant, Proceedings of the Fifth International Charles Parsons Turbine Conference, Advanced Materials for 21st Century Turbines and Power Plant, (Eds. A. Strang, W. M. Banks, R. D. Conroy, G. M. McColvin, J. C. Neal and S. Simpson) Institute of Materials, London 2000; 91-97.
- [3] Amorelli, A. and Howes, G. Impact of low carbon fuels on gas turbines design, Proceedings of the Seventh International Charles Parsons Turbine Conference, Power Generation in an Era of Climate Change, (Eds. A. Strang, W. M. Banks, G. M. McColvin, J. E. Oakey and R. W. Vanstone) Institute of Materials, London 2007; 9-12.
- [4] Ro, Y., Koizumi, Y. and Harada, H. High temperature tensile properties of a series of nickel-base superalloys on a γ/γ' tie line, Materials Science and Engineering A 1997; 223: 59-63.
- [5] Zhao, S., Xie, X., Smith, G.D. and Patel, S.J. Microstructural stability and mechanical properties of a new nickel based superalloy, Materials Science and Engineering: A 2003; 355: 96-105.
- [6] Murakumo, T., Kobayashi, T., Koizumi, Y. and Harada, H. Creep behavior of Ni-base single-crystal superalloys with various γ' volume fraction, Acta Materialia 2004; 52(12): 3737-3744.
- [7] Tancret, F. and Bhadeshia, H.K.D.H. (2003). An affordable creep-resistant nickel-base alloy for power plant, Proceedings of the 6th International Charles Parsons Turbine Conference, Engineering Issues in Turbine Machinery, Power Plant and Renewables, (Eds. A. Strang, R. D. Conroy, W. M. Banks, M. Blackler, J. Leggett, G. M. McColvin, S. Simpson, M. Smith, F. Starr and R. W. Vanstone) Institute of Materials, London 2003; 525-535.

- [8] Tancret, F., Bhadeshia, H. K. D. H. and MacKay, D. J. C. Design of a creep resistant nickel base superalloy for power plant applications. Part 1 – Mechanical properties modelling, *Materials Science and Technology*, 2003; 19: 283-290.
- [9] Weetham, G.W. *High Temp Alloys for Gas Turbines and Other Applications*, (Eds. Betz, et al.) Publisher: Reidel, Dordrecht, Holland, 1986.
- [10] Cummins, A.B. and Given, I.A. *SME Mining Engineering Handbook: Vol.1*, 2nd edition (H.L. Hartman, Ed.), Society for Mining, Metallurgy, and Exploration (Publisher), 1992.
- [11] Tawancy, H.M., Allam, I. M. and Abbas, N. M. Effect of Ni₃Nb precipitation on the corrosion resistance of Inconel alloy 625, *Journal of Materials Science Letters* 1990; 9: 343-347.
- [12] Reed, R. C. Numerical modelling of structure, properties and processing of nickel-based superalloys, *Proceedings of the Seventh International Charles Parsons Turbine Conference, Power Generation in an Era of Climate Change*, (Eds. A. Strang, W. M. Banks, G. M. McColvin, J. E. Oakey and R. W. Vanstone) Institute of Materials, London 2007; 89-97.
- [13] Zhao, S., Xie, X., Smith, G.D. and Patel, S.J. Gamma prime coarsening and age-hardening behaviors in a new nickel base superalloy. *Materials Letters* 2004; 58 (11): 1784–1787.
- [14] Caron, P. and Khan, T. Evolution of Ni-based superalloys for single crystal gas turbine blade applications, *Aerospace Science and Technology* 1999; 3(8): 513-523.
- [15] Barbosa, C., Nascimento, J.L., Caminha, I.M.V. and Abud, I.C. Microstructural aspects of the failure analysis of nickel base superalloys components, *Engineering Failure Analysis* 2005; 12: 348-361.
- [16] Kewther, M.A., Yilbas, B.S., and Hashmi, M.S.J. (2001). Tensile and fatigue testing of Inconel 617 alloy after heat treatment and electrochemical tests. *Industrial Lubrication and Tribology* 2001; 53 (3): 112-118.
- [17] Furillo, F.T., Davidson, J.M., Tien, J.K. and Jackman, L.A. The effects of grain boundary carbides on the creep and back stress of a nickel-base superalloy, *Materials Science and Engineering: A* 1979; 39: 267–273.
- [18] Mankins, W.L, Hosier, J.C and Bassford, T.H. Microstructure and phase stability of Inconel alloy 617. *Metallurgical and Materials Transactions B* 1974; 5 (12): 2579-2590.
- [19] Nickel, H. Characterization of metallic and ceramic high temperature materials for energy systems by means of atomic spectroscopy, *Pure and Applied Chemistry* 1993; 65 (12): 2481-2500.
- [20] He, L., Zheng, Q., Sun, X., Hou, G., Guan, H. and Hu, Z. (2005). M₂₃C₆ precipitation behaviour in a Ni-base superalloy M963. *Journal of Materials Science* 2005; 40 (11): 2959-2964.
- [21] Jo, T.S., Kim, G.S., Seo, Y.I., Ryu, W.S., and Do Kim, Y. Microstructure and high temperature mechanical properties of Inconel 617, (Eds. Kim H., Hojo J., Lee, S.W.) 8th International Symposium on Eco-Materials Processing and Design, Kitakyushu, Japan, Jan. 11-13, 2007, *Eco-Materials Processing And Design VIII* 2007; 411-414.
- [22] Gariboldi, E., Cabibbo, M., Spigarelli, S., and Ripamonti, D. Investigation on precipitation phenomena of Ni–22Cr–12Co–9Mo alloy aged and crept at high temperature, *International Journal of Pressure Vessels and Piping* 2008; 85: 63–71.
- [23] Ganesan, P., Smith; G.D., Yates, D.H. Performance of Inconel Alloy 617 in Actual and Simulated Gas Turbine Environments, *Materials and Manufacturing Processes* 1995; 10 (5): 925-938.
- [24] Ennis, P.J., Quadackers, W.J. and Schuster, H. The effect of selective oxidation of chromium on the creep strength of Alloy 617, *Materials Science and Technology* 1992; 8: 78-82.
- [25] Thermo-Calc Software AB (Version 4), <http://www.thermocalc.com>, SE-113 47: Stockholm, Sweden, August 2006.
- [26] Mazur, Z., Ramirez, A.L., Islas, J.A. J. and Amezcua, A.C. Failure analysis of a gas turbine blade made of Inconel 738LC alloy, *Engineering Failure Analysis* 2005; 12: 474–486.
- [27] Wusatowska-Sarnek, A.M., Blackburn, M.J. and Aindow, M. Techniques for microstructural characterization of powder-processed nickel-based superalloys, *Materials Science and Engineering A* 2003; 360 (1-2): 390-395.
- [28] Wu, Q., Song, H., Swindeman, R.W., Shingledecker, J.P. and Vasudevan, V.K, Microstructure of long-term aged IN617 Ni-base superalloy, *Metall. & Mater. Trans. A*. 2008; 39: 2569-2585